5650 *Inorg. Chem.* **2010**, *49*, 5650–5657
DOI: 10.1021/ic100398k

Inorganic Chemistry
Article

Pyrophosphate-Bridged Cu^{II} Chain Magnet: $\{[Na_3Cu(P_2O_7)(NO_3)]\cdot 3H_2O\}_n$

Rosana P. Sartoris,[†] Ricardo C. Santana,[‡] Ricardo F. Baggio,[§] Octavio Peña,[⊥] Mireille Perec,*[,¶] and Rafael Calvo*[,†]

[†]*Facultad de Bioquímica y Ciencias Biológicas, Universidad Nacional del Litoral and INTEC (CONICET-UNL), Güemes 3450, 3000 Santa Fe, Argentina,* [‡]*Universidade Federal de Goiás, Campus Samambaia, CP 131, 74001-970 Goiânia, Brazil,* [§]*Comisión Nacional de Energía Atómica, Avenida Gral Paz 1499, 1650 San Martín, Buenos Aires, Argentina,* [⊥]*Sciences Chimiques de Rennes, UMR 6226 CNRS, Université de Rennes 1, 35042 Rennes, France, and* [¶]*Facultad de Ciencias Exactas y Naturales, INQUIMAE, Universidad de Buenos Aires, Ciudad Universitaria, C1428EHA Buenos Aires, Argentina*

Received February 26, 2010

A $Cu^{II}\cdots Cu^{II}$ pyrophosphate-bridged compound of formula $\{[Na_3Cu(P_2O_7)(NO_3)]\cdot 3H_2O\}_n$ (**1**) has been characterized. X-ray diffraction measurements show that it crystallizes in the monoclinic space group $P2_1/m$, with unit cell dimensions $a = 7.2492(5)$ Å, $b = 8.2446(6)$ Å, $c = 9.9050(7)$ Å, $\beta = 107.123(1)°$, and $Z = 2$. The structure consists of chains of Cu^{II} cations at inversion symmetry sites bound to four equatorial oxygen atoms provided by two pyrophosphate anions halved by a symmetry plane and two axial oxygen atoms of nitrate anions. The molar magnetic susceptibility χ_0 of a powdered sample was measured in the temperature range $2\ K < T < 273\ K$, and an isothermal magnetization curve, $M(\mathbf{B}_0, T)$, was obtained at $T = 30$ K, with the magnetic field $\mathbf{B}_0$ between 0 and 5 T. Fitting a spin-chain model to the susceptibility data, we evaluate an antiferromagnetic exchange coupling $2J = -24.3(1)\ cm^{-1}$ (defined as $\mathcal{H}_{ex} = -2JS_iS_j$) between Cu^{II} neighbors. For any orientation of $\mathbf{B}_0$, single-crystal electron paramagnetic resonance (EPR) spectra obtained at 9.8 and 33.9 GHz at 300 K display a single signal having a **g** matrix with orthorhombic symmetry, arising from the merger produced by the exchange interaction of the resonances corresponding to the two rotated Cu^{II} sites. The **g** matrices of the individual molecules calculated assuming axial symmetry yielded principal values $g_{\parallel} = 2.367(1)$ and $g_{\perp} = 2.074(1)$ at both frequencies, indicating a $d_{x^2-y^2}$ ground-state orbital for the Cu^{II} ions. The angular variation of the EPR line width suggests exchange narrowing in a system with one-dimensional spin dynamics, as expected from the structure and susceptibility data. The results, discussed in terms of the crystal and electronic structures and of the spin dynamics of the compound, are compared with those obtained in other materials.

Introduction

The pyrophosphate anion $P_2O_7^{4-}$ (PPi) is known to play key biochemical roles in bioenergetic processes, driven by the hydrolysis of pyrophosphates into inorganic phosphates,[1] and in phosphocalcium metabolism.[2] Inorganic pyrophosphates are also of great interest in materials science, electrolytic, magnetic, and catalytic applications.[3] The usual synthetic route to such species is via high-temperature solid-state precursor methods or hydrothermal techniques.[4−6] Because of the lability of the tetraanion to hydrolysis, particularly in the presence of M^{II} cations,[7] synthetic strategies employing chelating ligands to control the self-assembly

*To whom correspondence should be addressed. E-mail: perec@qi.fcen.uba.ar (M.P.), calvo@fbcb.unl.edu.ar (R.C.).

(1) (a) Stryer, L. *Biochemistry*, 4th ed.; W. H. Freeman and Co.: New York, 2000. (b) Heikinheimo, P.; Pohjanjoki, P.; Helminen, A.; Tasanen, M.; Cooperman, B. S.; Goldman, A.; Baykov, A.; Lahti, R. *Eur. J. Biochem.* **1996**, *239*, 138–143.
(2) Ho, A. M.; Johnson, M. D.; Kingsley, D. M. *Science* **2000**, *289*, 265–270.
(3) Kasuga, T.; Terada, M.; Nogami, M.; Niinomi, M. *J. Mater. Res.* **2001**, *16*, 876–880.
(4) Erragh, F.; Boukhari, A.; Abraham, F.; Elouadi, B. *J. Solid State Chem.* **1995**, *120*, 23–31.
(5) Etheredge, K. M. S.; Hwu, S. J. *Inorg. Chem.* **1995**, *34*, 1495–1499.
(6) Yuen, P. S.; Collin, R. L. *Acta Crystallogr., Sect. B* **1974**, *30*, 2513–2516.
(7) (a) Heikinheimo, P.; Tuominen, V.; Ahonen, A. K.; Teplyakov, A.; Cooperman, B. S.; Baykov, A. A.; Lahti, R.; Goldman, A. *Proc. Natl. Acad. Sci. U.S.A.* **2001**, *98*, 3121–3126. (b) Zyryanov, A. B.; Shestakov, A. S.; Lahti, R.; Baykov, A. A. *Biochem. J.* **2002**, *367*, 901–906.
(8) Kruger, P. E.; Doyle, R. P.; Julve, M.; Lloret, F.; Niewenhuyzen, M. *Inorg. Chem.* **2001**, *40*, 1726–1727.
(9) (a) Ikotun, O. F.; Armatus, N. G.; Julve, M.; Kruger, P. E.; Lloret, F.; Nieuwenhuyzen, M.; Doyle, R. P. *Inorg. Chem.* **2007**, *46*, 6668–6674. (b) Ainscough, E. W.; Brodie, A. M.; Ranford, J. D.; Waters, J. M.; Murray, K. S. *Inorg. Chim. Acta* **1992**, *197*, 107–115. (c) Xu, J.-Y.; Tian, J.-L.; Zhang, Q.-W; Zhao, J.; Yan, S.-P.; Llao, D.-Z. *Inorg. Chem. Commun.* **2008**, *11*, 69–72. (d) Doyle, R. P.; Niewenhuyzen, M.; Kruger, P. E. *Dalton Trans.* **2005**, *23*, 3745–3750. (e) Ikotun, O. F.; Higbee, E. M.; Ouellette, W.; Lloret, F.; Julve, M.; Doyle, R. P. *Eur. J. Inorg. Chem.* **2008**, 5281–5286.

 Published on Web 04/28/2010

of Cu^{II} species in the presence of $(P_2O_7)^{4-}$ (e.g., 2,2′-bipyridine, 2-formylpyridine thiosemicarbazone, 2,2′-dipyridylamine, or 1,10-phenanthroline) allowed the isolation of a few Cu^{II} pyrophosphate-bridged hybrid compounds, which have been structurally and magnetically investigated.[8−11]

There is an exceedingly rich chemistry of Cu^{II} compounds with bonds to oxygen anionic ligands. Bleaney and Bowers first brought an explanation for the antiferromagnetic behavior of dimeric hydrated copper(II) acetate by their investigation of the single-crystal electron paramagnetic resonance (EPR) spectrum.[12] More recently, a number of structural and magnetic exchange studies have been reported for Cu^{II} trinuclear,[13] Cu^{II} tetranuclear,[14] and Cu^{II} pentanuclear[15] complexes with nonlinear arrays.

We report here a structural, magnetic, and single-crystal EPR study of a new polymeric material in which two inorganic anions (pyrophosphate and nitrate) occur within the same framework, embedded in a matrix of sodium countercations and water crystallization molecules. The electronic properties of the Cu^{II} ions and the magnetic behavior of the resulting polymeric spin-chain structure bridged by pyrophosphate anions are herein discussed.

Experimental Section

Materials. All chemicals were commercially available of analytical- or reagent-grade purity and were used as received. Water was purified by a Millipore Milli-Q system, yielding a resistivity of 18 MΩ cm^{-1}.

Synthesis of $\{[Na_3Cu(P_2O_7)(NO_3)]\cdot 3H_2O\}_n$ (1). $Cu(NO_3)_2\cdot 3H_2O$ (1 mmol, 0.241 g), glycylglycine (1 mmol, 0.075 g), and $Na_4P_2O_7$ (1 mmol, 0.266 g) were dissolved in warm water (150 mL) under stirring for 2 h and filtered while hot. The clear solution was maintained at 40 °C and pH = 7.5, and after several weeks, we obtained sky-blue rectangular prismatic crystals of **1**. Anal. Calcd for $CuNa_3H_6NO_{13}P_2$: H, 1.42; N, 3.32; O, 49.23; Cu, 15.04. Found: H, 1.40; N, 3.35; O, 49.15; Cu, 15.15. Main IR (KBr) cm^{-1}: 3589 (m), 3466 (w), 3407 (w), 3245 (w), 1667 (m), 1392 (s) [$\nu_{str}(NO_3)$], 1153 (s), 1082 (s), 1043 (w) [ν_{str}(Cu−O−P + O−P−O)], 892 (m), 768 (w), 601 (w). Raman (cm^{-1}): 1051 (s) [ν_{str}(Cu−O−P + O−P−O)].

Physical Techniques. Elemental analyses were performed on a Carlo Erba 1108 elemental analyzer. The copper content was determined on a Shimadzu AA6501 spectrophotometer. IR spectra were recorded as KBr pellets and as Nujol mulls on a Nicolet 510P FT-IR spectrophotometer with 64 scans and 4.0 cm^{-1} resolution. Raman spectra in the range of 400−1700 cm^{-1} were measured in backscattering geometry using a confocal microscope coupled to a single-stage spectrograph (Jobin Yvon XY 800) equipped with a liquid-nitrogen-cooled back-illuminated CCD detector. Elastic scattering was rejected with an edge filter. The 514-nm line of a continuous-wave argon ion laser (Coherent Innova 70c) was focused on the sample by means of a long-working-distance objective (20×; NA 0.35). Experiments were performed with laser power of ca. 10 mW at the sample, and acquisition times of ca. 10 s. Thermogravimetric analysis (TGA) measurements were carried out using a Shimadzu DTG 50 thermal analyzer under an air flow of 40 L min^{-1} at a heating rate of 5 °C min^{-1}. The purity of the product was checked by powder X-ray diffraction using monochromated Cu Kα radiation on a Philips X'Pert diffractometer.

Structural Methods. Single-crystal X-ray diffraction data were collected at 150(2) K with a Bruker CCD diffractometer, using graphite-monocromated Mo Kα radiation (λ = 0.710 73 Å). The programs *SMART*[16] and *SAINT*[17] were used as the driving and data integration software. For semiempirical absorption correction from equivalents, we used *SADABS*.[18] All calculations to solve the structures, refine the models, and obtain derived results were carried out with the computer programs *SHELXS97*,[19] *SHELXL97*,[19] and *SHELXTL*.[20] Full use of the CCDC package was made for searching in the CSD Database[21] and for crystal structure visualization.[22] The crystallographic data (excluding structure factors) are reported in the Supporting Information in this paper and deposited with the Cambridge Crystallographic Data Centre as CCDC 767240. Copies of the data can be obtained free of charge upon application to CCDC, 12 Union Road, Cambridge CB2 1EZ, United Kingdom [fax (44) 1223 336-033; e-maildeposit@ccdc.cam.ac.uk].

Magnetic Measurements. They were performed on finely powdered samples with a Quantum Design Squid magnetometer model MPMS XL5 using a calibrated gelatin capsule as a sample holder having a small diamagnetic contribution. The magnetic susceptibility was measured in the temperature interval 2 K < T < 273 K, with magnetic field $\mathbf{B}_0 = \mu_0\mathbf{H}$ = 200 mT (μ_0 is the permeability of the vacuum). A magnetization isotherm at 30 K was measured with 0 T < $\mathbf{B}_0$ < 5 T. In these measurements, the sample was cooled to the lowest T at zero field and $\mathbf{B}_0$ was turned on (zero-field cooling).

EPR Measurements. They were performed on single-crystal samples at room temperature using ER200 (9.8 GHz) and ESP300 (33.9 GHz) Bruker spectrometers, with standard Bruker cavities operating with 100 kHz field modulation. A crystal orientation was attained by gluing the *ab* growth face of the sample to a cleaved KBr single-crystal cubic holder, with the *b* axis parallel to one of the sides of the cube, which defines a *xyz* system of orthogonal axes, with *a*, *b*, and $c^* = a \times b$ crystal axes along the *x*, *y*, and *z* directions, respectively. The orientation of $\mathbf{B}_0$ was varied using a goniometer (9.8 GHz) or rotating the magnet (33.9 GHz). EPR measurements were performed with $\mathbf{B}_0$ at 10° (9.8 GHz) or 5° (33.9 GHz) intervals in the orthogonal planes *ab*, *bc**, and *ac** of the sample. The positions of the axes in the *ab* and *bc** planes were determined within ∼1° from the symmetry properties of the angular variation of the spectrum at the crystal axes.

Results and Discussion

An aqueous blue solution of $Cu(NO_3)_2$ and $Na_4P_2O_7$ in the presence of glycylglycine (1:1:1 molar ratio) at 40 °C and

(10) Doyle, R. P.; Kruger, P. E.; Moubaraki, B.; Murray, K. S.; Nieuwenhuyzen, M. *Dalton Trans.* **2003**, 4230–2037.
(11) Doyle, R. P.; Bauer, T.; Julve, M.; Lloret, F.; Cano, J.; Nieuwenhuyzen, M.; Kruger, P. E. *Dalton Trans.* **2007**, 5140–5147.
(12) Bleaney, B.; Bowers, K. D. *Proc. R. Soc. London* **1952**, *A214*, 451–465.
(13) (a) Clerac, R.; Cotton, F. A.; Dunbar, K. R.; Hillard, E. A.; Perukhinaet, M.; Smucker, B. W. *C. R. Acad. Sci, Chim.* **2001**, *4*, 315–319. (b) Cage, B.; Cotton, F. A.; Dalal, N. S.; Hillard, E. A.; Rakvin, B.; Ramsey, C. M. *J. Am. Chem. Soc.* **2003**, *125*, 5270–5271.
(14) (a) Kortz, U.; Nellutla, S.; Stowe, A. C.; Dalal, N. S.; van Tol, J.; Bassil, B. S. *Inorg. Chem.* **2004**, *43*, 144–154. (b) Kortz, U.; Nellutla, S.; Stowe, A. C.; Dalal, N. S.; Rauwald, U.; Danquah, W.; Ravot, D. *Inorg . Chem.* **2004**, *43*, 2308–2317.
(15) Nellutla, S.; van Tol, J.; Dalal, N. S.; Bi, L.-H.; Kortz, U.; Keita., B.; Nadjo, L.; Khitrov, G. A.; Marshall, A. G. *Inorg . Chem.* **2005**, *44*, 9795–9806.
(16) *Bruker, SMART-NT V5.624, Data Collection Software*; Siemens Analytical X-ray Instruments Inc.: Madison, WI, **2001**.
(17) *Bruker, SAINT-NT V6.22. Data Reduction Software*; Siemens Analytical X-ray Instruments Inc.: Madison, WI, **2001**.
(18) Sheldrick, G. M. *SADABS*; Bruker AXS Inc.: Madison, WI, **2002**.
(19) Sheldrick, G. M. *SHELXS 97 and SHELXL 97*; University of Göttingen: Göttingen, Germany, **1997**.
(20) *Bruker SHELXTL-NT*; Bruker AXS Inc.: Madison, WI, **2001**.
(21) (a) Allen, F. H. *Acta Crystallogr., Sect. B* **2002**, *B58*, 380–388. (b) Orpen, A. G. *Acta Crystallogr., Sect. B* **2002**, *58*, 398–406.
(22) (a) Macrae, C. F.; Edgington, P. R.; McCabe, P.; Pidcock, E.; Shields, G. P.; Taylor, R.; Towler, M.; van de Streek, J. *J. Appl. Crystallogr.* **2006**, *39*, 453–457. (b) Macrae, C. F.; Bruno, I. J.; Chisholm, J. A.; Edgington, P. R.; McCabe, P.; Pidcock, E.; Rodriguez-Monge, L.; Taylor, R.; van de Streek, J.; Wood, P. A. *J. Appl. Crystallogr.* **2008**, *41*, 466–470.

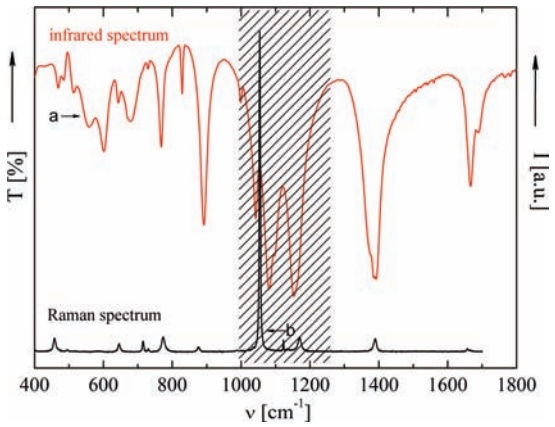

Figure 1. IR (a) and Raman (b) spectra of **1**. The strong IR band at 1392 cm^{-1} corresponds to NO^{3-}. The shadowed frequency region is the important range of the spectra.

pH = 7.5 yielded sky-blue rectangular prismatic crystals of **1** displaying *ab* growth faces. In the absence of glycylglycine in the reaction mixture, a blue-green powder was obtained. On the basis of a series of experiments under varied pH conditions, we verify that compound **1** is formed with good purity only within a small pH range of around 7.5. Glycylglycine does not coordinate to copper under these conditions, suggesting that it plays a buffering role (effective pH range of 7.5−8.9, pK_a = 8.20) during crystallization. Complex **1** is a stable crystalline solid and can be stored in a dry atmosphere at room temperature for extended periods of time. TGA shows a mass loss of 12.9% in the range of 117−244 °C, which corresponds to removal of three crystallization water molecules. IR and Raman bands of the solid material in the range of 1250−975 cm^{-1} are assigned to mixed stretching Cu−O−P and O−P−O modes in pyrophosphates on the basis of factor group effects.[5,23,24] The absence of coincidences for the majority of the IR and Raman bands (Figure 1) suggests a centrosymmetric structure of the material, as confirmed by the X-ray study.

Crystal Structure. Crystallographic data of **1** are given in Table 1 and selected bond distances and angles in Table 2. The structure consists of chains of copper cations in a distorted square-bipyramidal coordination related by C_2 rotations and inversion symmetry operations (Figure 2); copper atoms related by C_2 rotations are magnetically nonequivalent. The octahedral Cu^{II} ions present an equatorial plane parallel to (101) containing four oxygen atoms from two bridging pyrophosphate groups in the bis-bidentate coordination mode and two apical oxygen atoms from nitrate groups along the *b* axis. Cu^{II} neighbors along the chain, 4.122 Å apart, are connected through bridges: (i) $Cu1^{i}$−$O4^{ii}$−P2−O4 −Cu1, (ii) $Cu1^{i}$−$O2^{ii}$−P1−O2−Cu1, and (iii) $Cu1^{i}$−$O13^{i}$−Cu1 (symmetry codes are as in Table 2). The dihedral angle $Cu1^{i}$−$O13^{i}$−Cu1 is 108.66°, and angles O2−P1−$O2^{ii}$ and O4−P2−$O4^{ii}$ are 112.45 and 113.50°, respectively. The angle between the normals to the Cu^{II} basal planes of nearest-neighbor copper centers is 2α = 75.8(1)°. The sodium cations and the crystallization water molecules lie between chains, with the latter interacting by direct coordination with the sodium centers only and the former binding to the anions, pyrophosphates and nitrates, thus serving to bridge chains with each other into a tightly woven 3D network (Figure 3 and Table 3). Each chain is surrounded by six parallel neighbor chains, two along the *a* axes at 7.2492 Å, two along the *c* axes at 9.9050 Å, and the other two at 10.411 Å in the diagonal direction. Figure 4 shows the projection down the unique *b* axis, the chain direction, of the copper coordinaton polyhedra in a double lining, sodium interactions in a single lining, and

Table 1. Crystal Data and Structure Refinement for **1**

identification code	**1**
empirical formula	$Na_3Cu(P_2O_7)(NO_3)\cdot 3H_2O$
fw	422.51
temperature/K	150(2)
wavelength/Å	0.710 73
cryst syst	monoclinic
space group	$P2_1/m$
a/Å	7.2492(5)
b/Å	8.2446(6)
c/Å	9.9050(7)
α/deg	90
β/deg	107.123(1)
γ/deg	90
V/Å^3	565.75(7)
Z	2
D_c/g·cm^{-3}	2.480
μ/mm^{-1}	2.402
F(000)	418
cryst size/mm^3	0.18 × 0.14 × 0.12
θ range/deg	2.15−27.70
index ranges	$-9 \le h \le 9$, $-10 \le k \le 10$, $-12 \le l \le 12$
reflns: collcd, indep (R_{int}), obsd [$I > 2\sigma(I)$]	4550, 1331 (0.0136), 1309
no. of param	124
absorption	semiempirical from equivalents
max and min transmn	0.75 and 0.70
GOF on F^2	1.077
R indices [$I > 2\sigma(I)$]	R1 = 0.0181, wR2 = 0.0487
R indices (all data)	R1 = 0.0184, wR2 = 0.0489
largest peak and hole/e·Å^{-3}	0.418 and −0.344

Table 2. Selected Bond Lengths [Å] and Angles [deg] for **1**[a]

Cu−Cu^{i}	5.0740(5)	P2−O3	1.627(2)
Cu−O2	1.940(1)	Na1−O2W	2.336(1)
Cu−$O2^{i}$	1.940(1)	Na1−O1W	2.405(1)
Cu−$O4^{i}$	1.957(1)	Na1−$O4^{i}$	2.466(1)
Cu−O4	1.957(1)	Na1−$O5^{iii}$	2.5177(9)
Cu−$O13^{i}$	2.5371(9)	Na2−$O5^{iii}$	2.344(2)
Cu−O13	2.5371(9)	Na2−O1W	2.392 (1)
P1−O1	1.505(2)	Na2−$O1W^{ii}$	2.392(1)
P1−$O2^{ii}$	1.521(1)	Na2−$O12^{iv}$	2.430(2)
P1−O2	1.521(1)	Na2−$O11^{iv}$	2.535(2)
P1−O3	1.624(2)	Na2−$Na1^{ii}$	3.3910(9)
P2−O5	1.505(2)	Cu1−Na1	3.3486(7)
P2−$O4^{ii}$	1.524(1)	Cu1−$Na1^{i}$	3.3486(7)
P2−O4	1.524(1)	Na1−Na2	3.3910(9)
O2−Cu−$O2^{i}$	180.0	$O4^{i}$−Cu−$O13^{i}$	95.19(5)
O2−Cu−$O4^{i}$	86.80(4)	O4−Cu−$O13^{i}$	84.81(5)
$O2^{i}$−Cu−$O4^{i}$	93.20(4)	O2−Cu−O13	86.34(5)
O2−Cu−O4	93.20(4)	$O2^{i}$−Cu−O13	93.66(5)
$O2^{i}$−Cu−O4	86.80(4)	$O4^{i}$−Cu−O13	84.81(5)
$O4^{i}$−Cu−O4	180.0	O4−Cu−O13	95.19(5)
O2−Cu−$O13^{i}$	93.66(5)	$O13^{i}$−Cu−O13	180.00(6)
$O2^{i}$−Cu−$O13^{i}$	86.34(5)		

[a] Symmetry transformations used to generate equivalent atoms: (i) $-x+1, -y+2, -z$; (ii) $x, -y+{}^3/_2, z$; (iii) $x+1, y, z$; (iv) $-x+2, -y+2, -z+1$.

(23) Corbridge, D. E. C.; Lowe, E. J. *J. Chem. Soc.* **1954**, 493–502.
(24) Harcharras, M.; Ennaciri, A.; Rulmont, A.; Gilbert, B. *Spectrochim. Acta, Part A* **1997**, *53*, 345–352.

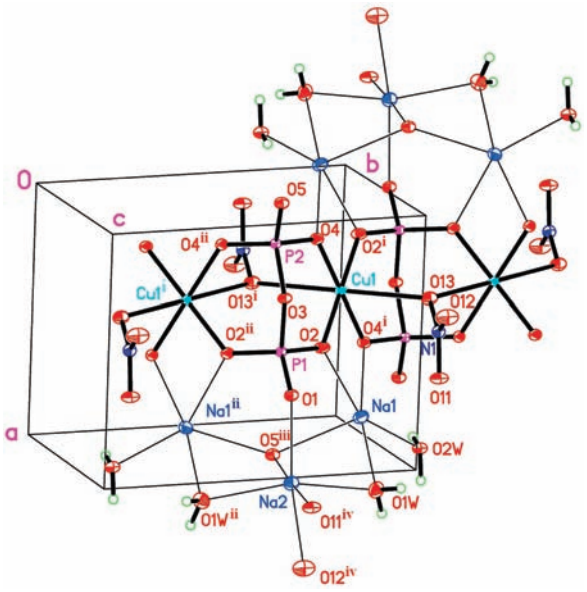

Figure 2. Molecular scheme of **1**, with displacement ellipsoids drawn at the 40% probability level. Na^+ interactions are drawn as thin lines. Symmetry codes are as given in Table 2.

Table 3. Lengths [Å] and Angles [deg] for Hydrogen Bonds for **1**[a]

D−H···A	*d*(D−H)	*d*(H···A)	*d*(D···A)	∠(DHA)
O1W−H1WA···O1^{iv}	0.840(9)	1.91(1)	2.747(2)	174(2)
O1W−H1WB···O12^{iii}	0.84(1)	2.32(2)	3.085(2)	151(2)
O2W−H2WA···O13^{iii}	0.86(1)	1.91(1)	2.746(2)	167(2)
O2W−H2WB···O5^{i}	0.85(1)	2.08(2)	2.856(2)	152(3)

[a] Symmetry transformations used to generate equivalent atoms: $-x+1, -y+2, -z$; (ii) $x, -y+{}^3/_2, z$; (iii) $x+1, y, z$; (iv) $-x+2, -y+2, -z+1$.

the three independent Cu···Cu paths linking different chains together in a thick lining. Bond lenghts and angles are consistent with the values reported for the related α-$Na_2Cu(P_2O_7)$,[4] $Na_2Cu(P_2O_7)$,[5] and $[Na_6Cu(P_2O_7)_2(H_2O)_2]\cdot 14H_2O$.[6]

Magnetic Properties. The isothermal magnetization curve, $M(\mathbf{B}_0,T)/N_{Av}$, of polycrystalline samples of **1** measured at $T = 30$ K is given in Figure S1 of the Supporting Information. The values increase linearly up to the maximum field, and no differences were observed between magnetization curves obtained with increasing or decreasing fields. As a consequence of the antiferromagnetic interactions (see later), the paramagnetic contributions to the low-temperature magnetization are very small, and the diamagnetic and temperature-independent (TIP) contributions of the sample are relatively important. So, these contributions were evaluated from the isothermal magnetization curve at 30 K and subtracted from the susceptibility data (see the Supporting Information). Figure 5 displays the molar susceptibility $\chi_0(T)$ and $T\chi_0(T)$ obtained at $\mathbf{B}_0 = 200$ mT as a function of the temperature, corrected for the TIP contributions as explained above. $\chi_0(T)$ exhibits a maximum value at $T_m = 22$ K and decreases with decreasing temperature, indicating antiferromagnetic interactions. The increase of $\chi_0(T)$ with decreasing T below 10 K is attributed to the presence of traces of mononuclear paramagnetic Cu^{II} (less than 1%). At high temperatures, $T\chi_0(T)$ displays a gradual increase with increasing T.

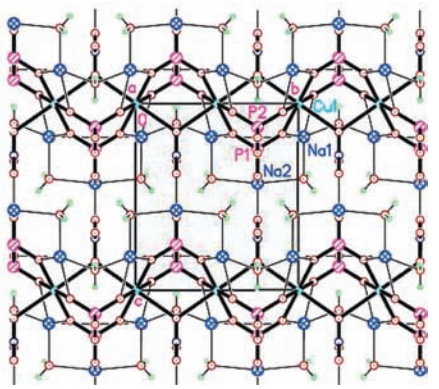

Figure 3. Projection of the structure down the *a* axis showing chains running along the *b* axis. Thin lines show their interconnection through interactions with Na^+ cations. The unit cell is shown in gray shadow.

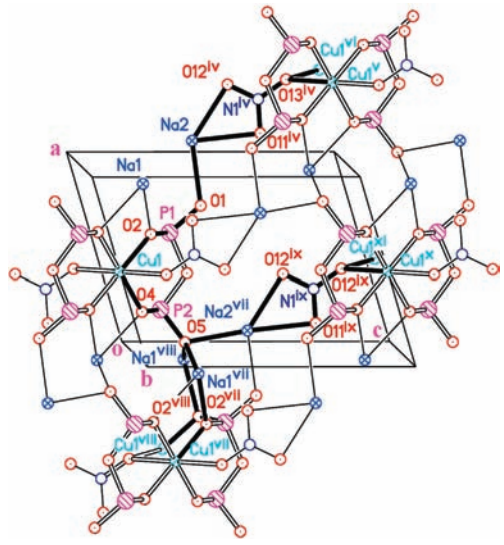

Figure 4. Projection down the chain direction, the unique *b* axis, showing in a double lining the copper coordinaton polyhedra, in a single lining sodium interactions, and in a heavy lining the Cu···Cu paths linking different chains together. The three independent paths starting from Cu1 are (a) Cu1−O4−P2−O5−[(Na1−O2−Cu1)^{vii}/−(Na1−O2−Cu1)^{viii}], (b) Cu1−O4−P2−O5−Na2^{vii}−([O11/O12]−N1−O13)^{ix}−[Cu1^{x}/Cu1^{xi}], and (c) Cu1−O2−P1−O1−Na2−([O11/O12]−N1−O13)^{iv}−[Cu1^{v}/Cu1^{vi}] ([.../...] stands for bifurcation). Water molecules are not shown for clarity. Symmetry codes: (iv) $2-x, 2-y, 1-z$; (v) $1+x, y, 1+z$; (vi) $-x, -0.5+y, 1-z$; (vii) $-1+x, y, z$; (viii) $-1+x, 1.5-y, z$; (ix) $1-x, 2-y, 1-z$; (x) $x, y, 1+z$; (xi) $1-x, -0.5+y, 1-z$.

EPR Data. A single resonance for the two magnetically nonequivalent copper ions in the lattice was observed for **1** at all field orientations. The position and peak-to-peak line width ΔB_{pp} of this resonance were obtained by least-squares fits of the observed spectra to Lorentzian derivative line shapes, whereas Gaussian line shapes rendered a much poorer fit to the data. Figures 6a,b and 7a,b display respectively the angular variations of the squared **g** value and of ΔB_{pp}, observed at room temperature in the planes *ab*, *bc**, and *ac** at 9.8 and 33.9 GHz, respectively. Similar values are obtained at both frequencies. The angular variation of the position of the single resonance is described by the spin Hamiltonian:

$$\mathcal{H} = \mu_B S\cdot\mathbf{g}\cdot\mathbf{B_0} \qquad (1)$$

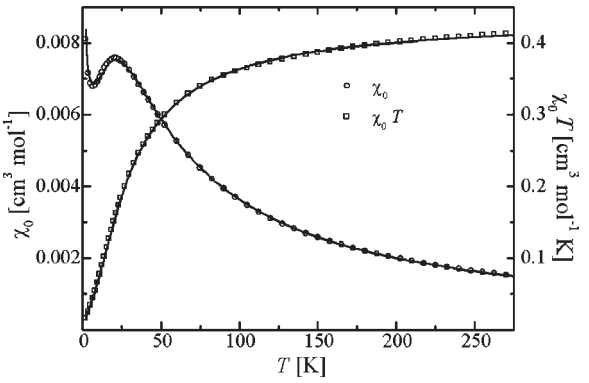

Figure 5. Experimental values of $\chi_0(T)$ and $T\chi_0(T)$ as a function of T. The solid lines were obtained by fitting eq 6 to the data.

where μ_B is the Bohr magneton, S is the effective spin operator of Cu^{II} ($S = {}^1/_2$), $\mathbf{g}$ is the crystal $\mathbf{g}$ matrix, and $\mathbf{B}_0 = B_0\mathbf{h} = B_0(\sin\theta\cos\varphi, \sin\theta\sin\varphi, \cos\theta)$. The components of the crystal $\mathbf{g}^2$ matrix given in Table 4 were calculated by fitting the function $g^2(\theta,\varphi) = \mathbf{h}\cdot\mathbf{g}\cdot\mathbf{g}\cdot\mathbf{h}$ to the experimental result. The calculated values (solid lines in Figure 6) are in good agreement with the data. The line widths observed in the *ab* and *bc** planes vary between 1.3 and 4.2 mT, with a maximum value along the direction of the chain (*b* axis, $\theta = \varphi = 90°$) and minima at 55−60° from the chain axis, close to the "magic angle" 54.75° (corresponding to $\theta = 35-40°$ and 140−145° in Figure 7a,b). The angular variation of the line width in the *ac** plane is much weaker.

Analysis and Discussion

Magnetic Behavior. Considering the structure of **1**, we explain the magnetic data proposing a linear spin chain model with nearest-neighbor exchange coupling $2J$ ($2J < 0$ for antiferromagnetic interactions). We calculated the magnetic susceptibility and the magnetization (Supporting Information) using the method of Bonner and Fisher,[25,26] which extrapolates the numerical results obtained for finite chains with N_s spins to infinite chains. Under an applied field $\mathbf{B}_0$ along z, they are described by

$$\mathscr{H} = -2J\sum_i^{N_s} S_i S_{i+1} + g\mu_B B_0 \sum_i^{N_s} S_{iz} \qquad (2)$$

where periodic conditions $S_{N_s+1} = S_1$ are imposed. The molar magnetization and the susceptibility can be written as[27,28]

$$M(B_0, T) = -\frac{N_{Av} g \mu_B \langle S_z\rangle}{N_s} \qquad (3)$$

$$\chi_0(x) = \frac{N_{Av} g^2 \mu_B{}^2}{N_s x|J|}[\langle S_z{}^2\rangle - \langle S_z\rangle^2] \qquad (4)$$

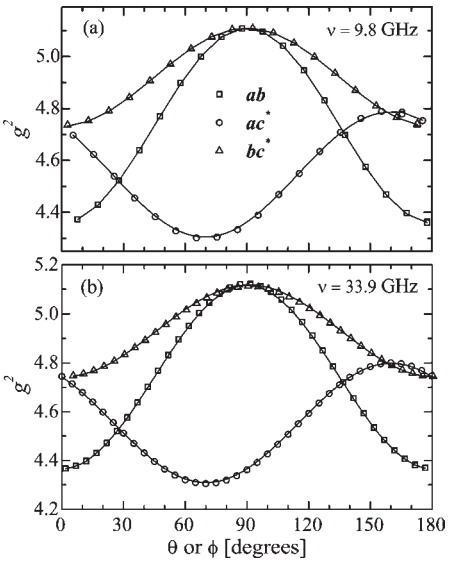

Figure 6. Angular variation of $g^2(\theta,\varphi)$ at (a) 9.8 GHz and (b) 33.9 GHz for B_0 applied in the *ab*, *ac** and *bc** crystal planes of **1**. The solid lines are calculated at each microwave frequency with the components of the $\mathbf{g}^2$ matrix, given in Table 4.

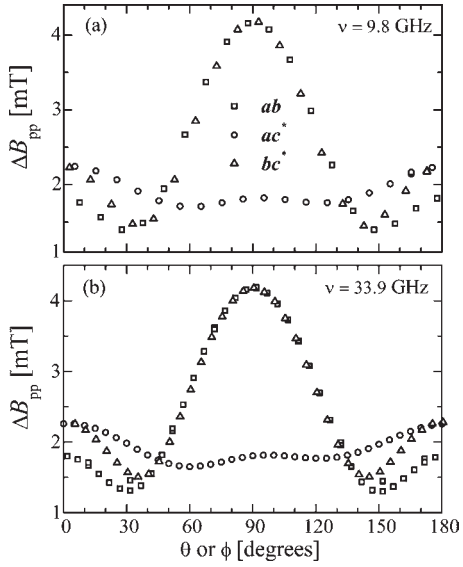

Figure 7. Angular variation of $\Delta B_{pp}(\theta,\varphi)$ at (a) 9.8 GHz and (b) 33.9 GHz for B_0 applied in the *ab*, *ac**, and *bc** crystal planes of **1**.

where N_{Av} is Avogadro's number, $\langle S_z\rangle$ and $\langle S_z{}^2\rangle$ are thermal averages of S_z and $S_z{}^2$ calculated for a spin chain with N_s spins under B_0 at temperature T, $x = k_B T/|J|$ is the reduced temperature, and $\langle S_z\rangle \sim 0$ at low B_0. At low x, $\kappa(x) = \chi(x)|J|/N_{Av} g^2 \mu_B{}^2$ should approach a finite nonvanishing value $(2\pi^2)^{-1}$ (see ref 29). Hall et al.[30] used the eigenvalues of chains of 11 spins to calculate a rational expression reproducing $\kappa(x)$ as a function of x, valid for $x > 0.5$, when $g\mu_B B_0 \ll k_B T$. This procedure has been used to fit data in spin-chain compounds with small exchange

(25) Bonner, J. C.; Fisher, M. E. *Phys. Rev. A* **1964**, *135*, 640–658.
(26) Griffiths, R. G. *Phys. Rev. A* **1964**, *135*, 659–660.
(27) Costa-Filho, A. J.; Nascimento, O. R.; Ghivelder, L.; Calvo, R. *J. Phys. Chem. B* **2001**, *105*, 5039–5047.
(28) Chagas, E. F.; Rapp, R. E.; Rodrigues, D. E.; Casado, N. M. C.; Calvo, R. *J. Phys. Chem. B* **2006**, *110*, 8052–8063.
(29) Griffiths, R. G. *Phys. Rev. A* **1964**, *133*, 768–775.
(30) Hall, J. W.; Marsh, W. E.; Weller, R. R.; Hatfield, W. E. *Inorg. Chem.* **1981**, *20*, 1033–1037. See also:Hatfield, W. E. *J. Appl. Phys.* **1981**, *52*, 1985–1990.

Table 4. Components of the Crystal $\mathbf{g}^2$ Matrix Obtained at 9.8 and 33.9 GHz by Least-Squares Fits of the Function $g^2(\theta,\phi) = (\mathbf{h}\cdot\mathbf{g}\cdot\mathbf{g}\cdot\mathbf{h})$ to the Data Displayed in Figure 6a,b[a]

	ν = 9.8 GHz	ν = 33.9 GHz
$(g^2)_{xx}$	4.3593(5)	4.3651(5)
$(g^2)_{yy}$	5.1095(5)	5.1176(5)
$(g^2)_{zz}$	4.7319(5)	4.7428(6)
$(g^2)_{xy}$	0	0
$(g^2)_{xz}$	−0.1595(5)	−0.1573(7)
$(g^2)_{yz}$	0	0
$(g^2)_1$	4.300(1)	4.308(1)
$(g^2)_2$	4.790(1)	4.7997(2)
$(g^2)_3$	5.109(7)	5.117 (1)
$\boldsymbol{a}_1$	[0.938(2), 0, 0.346(1)]	[0.9403(1), 0, 0.3403(1)]
a_2	[−0.346(2), 0, 0.346(2)]	[−0.3403(1), 0, 0.9403(1)]
a_3	[0, 1, 0]	[0, 1, 0]
$g_\parallel$	2.366(5)	2.368(8)
$g_\perp$	2.073(1)	2.075(1)
θ_m (deg)	54.8(1)	54.7(1)
φ_m (deg)	74.9(1)	75.2(1)
2α (deg)	75.8(1)	75.8(1)

[a] The eigenvectors of $\mathbf{g}^2$, the angles 2α between the normals n_A and n_B to the planes of ligands to Cu^{II} ions in lattice sites A and B, and (θ_m, ϕ_m) for the orientation of the direction of $g_\parallel$ for site A in the lattice, calculated from the EPR data, are included.

interactions and $x \geq 0.5$.[31] However, our results at low T correspond to $x \sim 0.1$, where Hall's method is not valid and has to be revised. Thus, using the eigenvalues of chains with up to 16 spins[32] and the asymptotic limit of $\kappa(x)$ for $x \rightarrow 0$,[29] we calculated a rational expression that replaces the result of Hall et al.[30] and reproduces well the reduced susceptibility for $x \geq 0.1$. If $\chi_0(x) = (N_{Av}g^2\mu_B{}^2/|J|)\kappa(x)$, then

$$\kappa(x) = \frac{1}{N_s x}\langle S_z{}^2\rangle = (0.05066 - 0.02380x + 0.11360x^2 - 0.09830x^3 + 0.30900x^4)/(1 - 0.08517x + 1.51000x^2 + 1.12480x^3 + 0.85950x^4 + 1.23650x^5) \quad (5)$$

For $x \rightarrow 0$, $\kappa(x) = 0.05066 = (2\pi^2)^{-1}$.[29] Considering the contribution to the susceptibility of a fraction ρ of mononuclear paramagnetic impurities, which are important at low T,[33] we least-squares-fitted eq 6

$$\chi_{exp}(T) = (1-\rho)\chi_0(T) + \rho \lim_{B_0 \rightarrow 0} \frac{\frac{1}{2}N_{Av}g\mu_B \tanh(g\mu_B B_0/2k_B T)}{B_0} \quad (6)$$

to the data in Figure 5 to obtain $g = 2.16$, $2J = -24.3(1)$ cm^{-1}, and $\rho = 0.0080(1)$ (agreement factor $R = 0.9997$). This value of $2J$ is similar to $2J = -24\,cm^{-1}$ estimated from the position of the peak value of $\chi_0(T)$ using $k_BT/|J| = 1.282$.[25] The solid lines in Figure 5, calculated with eq 6, agree with the experimental result.

Our analysis of the magnetic susceptibility assumes a 1D behavior with chains along the *b* axis. If the coupling between coppers in parallel neighboring chains were not negligible, 2D or eventually 3D magnetic behavior could be expected. In the structural data of **1**, the three chemical bridges i, ii, and iii connecting Cu^{II} ions along the *b* axis (Figure 3) have total lengths of 6.922, 6.962, and 5.074 Å, much shorter than the pathways connecting coppers in neighboring chains, described as a−c in the caption to Figure 4 and having total lengths of approximately 11.827, 14.906, and 14.970 Å. These lengths and the higher complexity of the interchain paths indicate that the most important superexchange pathways between Cu^{II} ions in **1** are along the chains, consistent with our analysis of the susceptibility data.

Studies of the related dimeric species $\{[(bipy)Cu(H_2O)]_2(\mu\text{-}P_2O_7)\cdot 7H_2O\}$ with the pyrophosphate group also acting as a bis-bidentate ligand defining two six-membered chelate rings at a Cu···Cu distance of 4.646 Å have been adjusted with $g = 2.09$ and $2J = -20\ cm^{-1}$.[8] The value of the exchange coupling between Cu···Cu neighbors obtained for **1** is smaller than $2J = -12(1)\ cm^{-1}$ calculated from ^{31}P NMR data for the related pyrophosphate $Na_2Cu(P_2O_7)$,[34] using a 2D model. In that compound, symmetry-related copper atoms connected by a bis-bidentate pyrophosphate ligand give rise to chains along the *c* axis with a Cu···Cu distance of 6.929 Å. These chains are arranged in layers parallel to the *ac* plane, with the free spaces between the layers occupied by sodium cations. Within these layers, Cu^{II} ions of neighboring chains are connected by paths containing five diamagnetic atoms (Cu−O−P−O−Na−O−Cu) with a total Cu···Cu length of 9.619 Å. Meanwhile, Cu^{II} ions in parallel layers are linked by two identical paths containing three diamagnetic atoms (Cu−O−Na−O−Cu), with a length of 8.936 Å giving rise to a 3D lattice. These structural differences support the 2D spin dynamic reported in $Na_2Cu(P_2O_7)$.[34,35] The difference in the magnitudes of $2J$ for the two compounds is significant; however, the support of the models on which the calculations are based renders a straightforward interpretation of the differences rather doubtful.

EPR. Crystal and Molecular g Matrices. Because copper ions in **1** occupy two magnetically nonequivalent sites along the *a* axis, Cu1[i] and Cu1, related by a C_2 rotation around the *b* axis, two resonance lines should be observed for most orientations of $\mathbf{B}_0$. However, only one line is observed as a consequence of the exchange interactions between neighboring rotated Cu^{II} ions, which appears to be large enough to merge their resonances.[36] From the calculated crystal **g** matrix having orthorhombic symmetry (Table 4), we evaluated the molecular $\mathbf{g}_A$ and $\mathbf{g}_B$ matrices (differing in a C_2 rotation around *b*), following a procedure described previously[37] that assumes axial

(31) (a) Calvo, R.; Passeggi, M. C. G.; Novak, M. A.; Symko, O. G.; Oseroff, S. B.; Nascimento, O. R.; Terrile., M. C. *Phys. Rev. B* **1991**, *43*, 1074–1083. (b) Calvo, R.; Levstein, P. R.; Castellano, E. E.; Fabiane, S. M.; Piro, O. E.; Oseroff, S. B. *Inorg. Chem.* **1991**, *30*, 216–220. (c) Calvo, R.; Steren, C. A.; Piro, O. E.; Rojo, T.; Zuñiga, F. J.; Castellano, E. E. *Inorg. Chem.* **1993**, *32*, 6016–6022. (d) Calvo, R.; Passeggi, M. C. G.; Moreno, N. O.; Barberis, G. E.; Chaves, A. B.; Torres, B. C. M.; Lezama, L.; Rojo, T. *Phys. Rev. B* **1999**, *60*, 1197–1203.
(32) Fabricius, K.; Lôw, U.; Mutter, K.-H.; Ueberholz, P. *Phys. Rev. B* **1991**, *44*, 7476–7485See also ref 24.
(33) Kahn, O. *Molecular Magnetism*; VCH: New York, 1993.
(34) Nath, R.; Mahajan, A. V.; Büttgen, N.; Kegler, C.; Hemberger, J.; Loidl, A. *J. Phys.: Condens. Matter* **2006**, *18*, 4285–4294.
(35) Salunke, S.; Singh, V. R.; Mahajan, A. V.; Dasgupta, I. *J. Phys.: Condens. Matter* **2009**, *21*, 025603.
(36) Calvo, R. *Appl. Magn. Reson.* **2007**, *31*, 271–299.
(37) (a) Calvo, R.; Mesa, M. A. *Phys. Rev. B* **1979**, *28*, 1244–1248. (b) Calvo, R.; Mesa, M. A.; Oliva, G.; Zukerman-Schpector, J.; Nascimento, O. R.; Tovar, M.; Arce, R. *J. Chem. Phys.* **1984**, *81*, 4584–4591.

symmetry for the copper molecule. The principal g factors $g_{\|}$ and $g_{\perp}$, the polar and azimuthal angles θ_m and φ_m describing the direction along which $g_{\|}$ occurs for copper in sites Cu1, and the angle 2α between the normals to the equatorial planes of sites Cu1^{i} and Cu1 are included in Table 4. The parameters θ_m, φ_m, and 2α calculated at both frequencies are in good agreement with the crystallographic values $\theta_c = 57.0(1)°$, $\varphi_c = 71.4(1)°$, and $2\alpha_c = 75.8(1)°$, supporting the assumption of axial symmetry and indicating that the ground state is well described by a $d_{x^2-y^2}$ orbital.[38]

Line Width. The temperature variation of the magnetic susceptibility is a good indicator of the dimensionality of the magnetic properties, which are mainly related to the ratio between the exchange couplings connecting the metal ions along different crystal directions.[39] The angular variation of the EPR line width is also used as a dimension indicator, related to the dimensionality of the spin dynamics, i.e., the diffusive propagation of the spin excitations in the material.[40−42]

The main contributor to the EPR line width ΔB_{pp} arises from the (anisotropic) magnetic dipole−dipole interactions between Cu^{II} ions, which can be calculated using the second moment method.[43] When the secular term is the main contributor, line widths observed at different microwave frequencies are very similar, as occurs in **1** (Figure 7a,b), and the second moment M_2 may be expressed as follows:[43]

$$M_2 = \frac{3}{4} g^4 \mu_B{}^4 S(S+1) \sum_k \frac{(1 - 3\cos^2\theta_{jk})^2}{r_{jk}{}^6} \qquad (7)$$

where r_{jk} is the distance between copper ions at sites j and k and θ_{jk} is the angle between r_{jk} and $\mathbf{B}_0$. Using the crystallographic data and an isotropic value $g = 2.156$, obtained from the EPR data, we calculated M_2 as a function of the orientation of $\mathbf{B}_0$, adding eq 7 over the contributions of all spins in the lattice. Because M_2 is mainly proportional to r_{ij}^{-6} between Cu^{II} neighbors, the contribution of the dipolar interaction between the copper ions in two neighboring chains at 7.249 Å along the a axis is much smaller than the contributions of the intrachain interactions. The line widths $\Delta B_{pp} = (1/g\mu_B)(M_2)^{1/2}$ calculated by this method are more than 15 times larger than the experimental result, reflecting the effect of the exchange interactions between Cu^{II} ions, which modulate the dipolar interaction and narrow the line,[44−46] in a process that is highly dependent on the dimensionality of the spin system.[40−47] For 3D spin dynamics, the exchange-narrowed line width can be obtained using the expression[44−46]

$$(\Delta B_{pp})_{3D} = \frac{1}{g\mu_B} \frac{M_2}{|2J|} \qquad (8)$$

However, considering the structural data of **1** and the 1D static magnetic behavior indicated by the susceptibility data, the observed line width should reflect the much slower narrowing effect expected for 1D spin dynamics. Gatteschi et al.[43−48] proposed for the line width of a spin chain

$$(\Delta B_{pp})_{1D} = \frac{1}{g\mu_B} \left[\frac{(M_2)^2}{|2J|} \right]^{1/3} \qquad (9)$$

The symbols in Figure 8 display the experimental values of the line width in the planes *ab* and *bc*, containing the chain direction ***b*** and displaying the largest angular variation. The lines in this figure display the values obtained by fitting eqs 8 and 9 to these data, using the values of the second moment M_2 obtained with eq 7, and the structural information. In these fittings, we assumed that the observed line width is the sum of the exchange-narrowed dipolar contributions of eq 8 or 9, plus a smaller constant contribution ΔB_0 attributed to other sources of line width, such as those produced by structural imperfections. Because these contributions are uncorrelated, we fitted the expressions

$$(\Delta B_{pp})_{exp} = [(\Delta B_{pp})_{1D}{}^2 + \Delta B_0{}^2]^{1/2} \quad \text{or}$$

$$(\Delta B_{pp})_{exp} = [(\Delta B_{pp})_{3D}{}^2 + \Delta B_0{}^2]^{1/2}$$

to the line-width data. The mean-square deviations of each result, σ_{1D} and σ_{3D}, included in Figure 8, indicate a better agreement for the 1D model (eq 9). Nevertheless, the

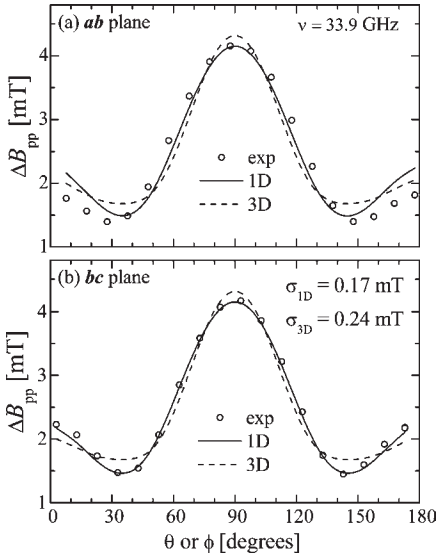

Figure 8. EPR line width observed in the *ab* and *bc** planes (symbols) is 33.9 GHz. The lines are obtained with 3D and 1D models for the spin dynamics, as explained in the text. The 1D model (eq 8) gives a better agreement with the shape of the angular variation.

(38) Zweiger, H. J.; Pratt. G. W. *Magnetic Interactions in Solids*; Oxford University Press: London, 1973.
(39) de Jongh, L. J.; Miedema, A. R. *Adv. Phys.* **1974**, *23*, 1–260. Reprinted: *Adv. Phys.* **2001**, *50*, 947−1150.
(40) Dietz, R. E.; Merritt, F. R.; Dingle, R.; Hone, D.; Silbernagel, B. G.; Richards, P. M. *Phys. Rev. Lett.* **1971**, *26*, 1186–1188.
(41) Richards, P. M.; Salamon, M. B. *Phys. Rev. B* **1974**, *9*, 32–45.
(42) Richards,P. M. *Local Properties at Phase Transitions*; Editrice Compositori: Bologna, Italy, 1975; pp 539−606.
(43) Van Vleck, J. H. *Phys. Rev.* **1948**, *74*, 1168–1183.
(44) Anderson, P. W.; Weiss., P. R. *Rev. Mod. Phys.* **1953**, *25*, 269–276.
(45) Anderson, P. W. *J. Phys. Soc. Jpn.* **1954**, *9*, 316–339.
(46) Pake, G. E. *Paramagnetic Resonance, An Introductory Monograph*; Benjamin: New York, 1962; Chapter 7.
(47) Gatteschi, D.; Sessoli, R. *Magn. Reson. Rev.* **1990**, *15*, 1–45.
(48) Bencini, A.; Gatteschi, D. *Electron Paramagnetic Resonance of Exchange Coupled Systems*; Springer: Berlin, 1990.

improvement of the shape of the 1D fit over the 3D fit is not large enough to ensure pure 1D spin dynamics. The values of J obtained with the fittings are $\sim$1 cm^{-1} (25 times smaller than the value obtained from the susceptibility data) for the 3D fit and $\sim$230 cm^{-1} for the 1D fit (10 times larger than that value). This result reminds us that these models are valid for nearly perfect 3D (isotropic) or 1D (unidirectional) behavior, and the spin dynamics of **1** differ from either of these two limits. Thus, they do not allow us to obtain the magnitude of the exchange interaction but only predict approximately the shape of the angular variation of the line width.

Conclusions

We report herein a new copper(II) pyrophosphate chain magnet, **1**, isolated from an aqueous solution of $Cu(NO_3)_2$ and $Na_4(P_2O_7)$, buffered with glycylglycine at pH = 7.5. The Cu^{II} ions in the structure form spin chains in an extended linear structure constructed by alternating CuO_6 and P_2O_7 units characterized by bis(pyrophosphate) chelates. The magnetic susceptibility is interpreted with a spin-chain model that reveals the existence of a relatively strong antiferromagnetic coupling between copper neighbors in the chain, $2J = -24.3(1)$ cm^{-1} (defined as $\mathcal{H}_{ex} = -2JS_iS_j$). Detailed single-crystal EPR experiments at two microwave frequencies show that the single resonance observed for any orientation of the field is a result of the collapse of the two resonances expected from the structural data, produced by the exchange interactions. The spin Hamiltonian parameters of the individual copper ions calculated from the EPR data under the hypothesis of axial symmetry agree with the crystal structure and give information about the electronic structure of the Cu^{II} ions. The angular variation of the EPR line width supports a slow diffusive spin dynamics along the chain, yet the exchange coupling giving rise to this particular spin dynamics cannot be evaluated using the existing models of line narrowing.

Acknowledgment. The authors acknowledge ECOS Sud A05E01, the France−Argentina Binational Cooperation Project that made this collaboration possible. This work was supported by PIP 5274 from CONICET and PICT 25409 BID/728/OC/AR in Argentina and by CNPq in Brazil. R.C. and M.P. are members of CONICET.

Note Added after ASAP Publication. This paper was published on the Web on April 28, 2010, with incorrect y-axis values in Figure 7. The corrected version was reposted on May 13, 2010. Additional corrections were received for Figure 7 and the second sentence of the caption was removed. The corrected version was reposted on May 19, 2010.

Supporting Information Available: X-ray crystallographic data in CIF format and isothermal magnetization curves obtained at 30 K with $\mathbf{B}_0$ between 0 and 5 T. This material is available free of charge via the Internet at http://pubs.acs.org.